IOP Conference Series: Earth and Environmental Science

PAPER • **OPEN ACCESS**

Numerical simulation of pressure distribution in a walking-beam type reheating furnace

To cite this article: Chaoxiang Li *et al* 2020 *IOP Conf. Ser.: Earth Environ. Sci.* **467** 012025

IOP Conf. Series: Earth and Environmental Science **467** (2020) 012025 doi:10.1088/1755-1315/467/1/012025

Numerical simulation of pressure distribution in a walking-beam type reheating furnace

Chaoxiang Li, Yajun Huang[1], Junbo Sun, Yang Ni and Linlin Lu

School of Energy and Environment, Anhui University of Technology, Ma'an shan 243002, China

[1] Email: yajunhuang2017@163.com

Abstract. Numerical simulation of pressure distribution in a walking-beam reheating furnace was accomplished using FLUENT software. The effect of partition walls in the preheating zone on the flow field and pressure distribution in the reheating furnace was studied. The numerical results show that the partition walls in the preheating zone have an important influence on pressure distribution and temperature distribution in the reheating furnace. In order to improve the pressure distribution and the temperature uniformity in the reheating furnace, the partition walls in the preheating zone were retrofitted. After the partition walls retrofitting, the pressure distribution and the temperature distribution in the reheating furnace were improved. The heating efficiency of the reheating furnace was improved. Therefore, numerical results have great significance for improving pressure distribution and temperature distribution in the reheating furnace.

1. Introduction

Large continuous reheating furnaces are employed in the steel plants for heating up slabs or billets to an appropriate hot rolling temperature. During the reheating process, the furnaces not only consume a lot of energy, but also produce a lot of CO_2 and gaseous pollutants. This exacerbates the greenhouse effect and environmental pollution. Therefore, reducing the production of CO_2 and gaseous pollutants in reheating furnaces has attracted attention. Since the production of CO_2 and gaseous pollutants is positively correlated with energy consumption, reducing energy consumption can reduce the production of CO_2 and gaseous pollutants. Thus, much effort has been placed on reducing the energy consumption in reheating furnaces.

In order to reduce energy consumption of reheating furnaces, the heating efficiency of reheating furnaces needs to be improved. There are many factors that affect the thermal efficiency of reheating furnaces, which include the distribution of the hot gas in the furnace, type of fuel, location of slabs, residence time of slabs, thermal properties of slabs, geometry of the slab supporting systems, and etcetera. At present, the influence of some factors on the thermal efficiency of reheating furnaces has been studied. For example, Han et al. [1] numerically verified that the use of oxy-fuel combustion instead of air-fuel combustion can increase the efficiency of reheating furnaces. Han et al. [2] also studied the effects of various fuel feeding rates on the thermal performance of reheating furnaces. JakličA et al. [3] investigated the effect of space between billets on the productivity of a continuous walking-beam reheating furnace. Some scholars [4-6] proposed the optimal residence time of slabs in the reheating furnace. Jang and Huang [7-8] optimized the heating pattern of slabs and achieved the energy saving of reheating furnaces. Emadi et al. [9] studied the heating characteristics of the billet in a walking beam reheating furnace. However, the influence of the distribution of hot gas in the reheating furnace on the thermal efficiency of the reheating furnace has not been widely studied. Since hot gas in the reheating furnace plays a deterministic role during the slab heating process. It is imperative to study the distribution of hot gas in the reheating furnace. The distribution of hot gas is mostly affected by the pressure in the reheating furnace. Therefore, the focus of this research is the pressure distribution in the reheating furnace.

In the 1980s and 1990s, Chinese researchers studied the law of the pressure distribution along the furnace length direction of reheating furnaces. The law was used to guide the operation of reheating furnaces which achieved a good energy-saving effect. However, with the development of the steel industry, the structure of reheating furnaces has been significantly changed, which makes the previous studies by former researchers that are no longer applicable to the existing reheating furnace. Therefore, it is necessary to study the pressure distribution in reheating furnaces to meet the new expectations.

Recently computational fluid dynamics (CFD) simulations have become an important tool to study flow and heat transfer characteristics in industrial furnaces [10-12] and CFD software fluent was widely used in the research of the reheating furnace [12-14]. In this paper, the emphasis is the numerical simulation of the effect of different partition walls in the preheating zone on the distribution of the flow field, the pressure distribution in the reheating furnace using the fluent software, followed by experimental measurement the slab temperature in the reheating furnace, and compared the experimental results with the simulation results.

2. Configuration of the reheating furnace

In this study, the furnace is a walking beam reheating furnace in Nanjing Iron and Steel Corporation in China as shown in Figure 1. The x-axis is the length direction of the furnace. Slabs move in the positive direction of the x-axis. The movement of the hot gas is along the negative direction of the x-axis. The direction of the y-axis is the height direction of the furnace. Hence, the direction of the z-axis is the width direction of the furnace. Since the reheating furnace is symmetric with respect to the z = 0 plane, the calculation can use the half section of the furnace.

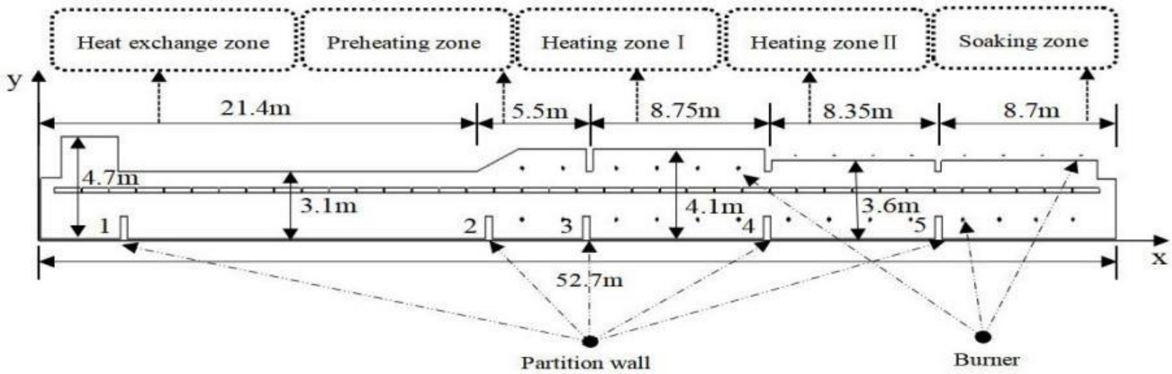

Figure 1. Configuration of the reheating furnace.

The reheating furnace includes five zones: the heat exchange zone, the preheating zone, the heating zone I, the heating zone II, and the soaking zone. The length of the furnace is 52.7m, including 21.4m of the heat exchange zone, 5.5m of the preheating zone, 8.75m of the heating zone I, 8.35 of the heating zone II, and 8.7m of the soaking zone. The width of the furnace is 11.7m and the height of the furnace is shown in Figure 1. The black spots in Figure 1 represent the positions of the burners in the reheating furnace. The furnace is equipped with 104 burners as listed in Table 1. The fuel used in this study is high coke mixed gas, its composition in volume is: 39.5% N_2, 20.4% H_2, 19.7% CO, 8.6% CO_2, 8.5% CH_4, 2.3% H_2O, 0.7% C_2H_4, and 0.3% O_2. The heat of combustion of the fuel is 8172 kJ/m^3 at 273.15K and 1 atm. The temperature of the inlet air is 350°C and the high coke mixed gas temperature is 250°C. The fuel consumption of the furnace under standard conditions is 24000 Nm^3/h and the throughput of the furnace is 350t/h. At the bottom of the furnace, there are five partition walls including the partition wall 1, the partition wall 2, the partition wall 3, the partition wall 4 and the partition wall 5. It is worth noting here that the partition walls in case 1 and case 2 are different. In case 1, the height of the partition wall is 1050mm. The partition wall is not connected with both side furnace walls and the distance between the partition wall and the side furnace wall is 400mm. In case 2, the height of the partition wall also is 1050mm. However, the structures of the partition wall 2 and the partition wall 3 have changed. In case2, the partition wall 2 and the partition wall 3 connect with both side furnace walls. The middle sections of the partition wall 2 and the partition wall 3 were removed and the length of the removed partition wall is 6000mm.

3. Numerical model and test method

3.1. Governing equations

For the simulations, the flue gas in the furnace was assumed to be at steady-state and incompressible flow. The flue gas flow in the furnace was calculated using standard k-ε equations given in Eqs.(5) and (6). The equations can be found in reference [15]:

Continuity equation:

$$\frac{\partial u_i}{\partial x_\mathrm{i}} = 0 \tag{1}$$

where ρ is the fluid density, u_i is velocity.

Momentum equation:

$$\frac{\partial}{\partial x_i}(\rho u_i u_j) = -\frac{\partial p}{\partial x_j} + \frac{\partial}{\partial x_i}\left[\mu_{eff}\left(\frac{\partial u_i}{\partial x_j} + \frac{\partial u_j}{\partial x_i}\right)\right] + \rho g_i + F_j \tag{2}$$

where p is the pressure, $\mathrm{F_j}$ is the body force.

where

$$\mu_{eff} = \mu + \mu_t \tag{3}$$

$$\mu_t = \rho c_u \frac{k^2}{\varepsilon} \tag{4}$$

where c_u is 0.09.

Turbulent kinetic energy equation: k

$$\rho u_i \frac{\partial k}{\partial x_i} = \frac{\partial}{\partial x_i}\left[\left(\mu + \frac{\mu_t}{\sigma_k}\right)\frac{\partial k}{\partial x_i}\right] + G - \rho\varepsilon \tag{5}$$

Turbulent dissipation equation ε :

$$\rho u_i \frac{\partial \varepsilon}{\partial x_i} = \frac{\partial}{\partial x_i}\left[\left(\mu + \frac{\mu_t}{\sigma_\varepsilon}\right)\frac{\partial \varepsilon}{\partial x_i}\right] + \frac{c_1\varepsilon}{k}G - c_2\rho\frac{\varepsilon^2}{k} \tag{6}$$

where, c_1, c_2, σ_k, and σ_ε are constants, which are equal to 1.44, 1.92, 1.0 and 1.3, respectively.

where

$$G = \mu_t \frac{\partial u_i}{\partial x_j}\left(\frac{\partial u_i}{\partial x_j} + \frac{\partial u_j}{\partial x_i}\right) \tag{7}$$

3.2. Boundary conditions

The inlet sizes and the flows of the burners are shown in Table 1. All inlets at the burners were modeled by the velocity-inlet conditions. The outlets of the furnace were modelled by the pressure-outlet conditions. The furnace walls and slabs are adiabatic walls. The walls of the models were stationary walls and the boundary conditions of walls were no-slip conditions.

Table 1. Inlet sizes and flows of burners.

Zone	Type	Number	D_{air}/mm	D_{fuel}/mm	Q_{air}/(m^3/h)	Q_{fuel}/(m^3/h)
Preheating zone	Side burners	4	148	74	27.88	0
		4(bottom)	148	74	41.20	0
Heating zone I	Side burners	8	148	74	109.28	84
		8(bottom)	148	74	119.05	94
Heating zone II	Side burners	8	148	74	73.48	58.82
	Top burners	32	88	40	62.64	62.66
Soaking zone	Side burners	8	148	74	66.21	49.48
	Top burners	32	88	40	12.52	14

3.3. Test method

A "black box" temperature recorder was used to take the slab temperature in this experiment. The temperature recorder consists of three parts: the thermocouple temperature sensor, data recorder and high-temperature water tank.

A QSTE420TM slab was chosen as the experimental slab, and the dimension of the slab is 10000mm (length)×1500mm (width)×230mm (thickness). Before the experiment, three holes at different depths were drilled from the slab top surface vertically down at the two ends and the middle part of the slab. The bottoms of these holes represent the upper surface, middle thickness, and the lower surface of the slab, respectively. Then the thermocouples were inserted to these holes and fixed on the upper surface of the slab. The other end of the thermocouples was connected to the data recorder. The data recorder was put into the high temperature water tank, and the high temperature water tank was fixed on the slab. The experimental slab with the above setup was put into the reheating furnace for heating. At the end of reheating process, the experimental slab was removed from the furnace, the temperature data of the slab was extracted from the data recorder for analysis.

4. Results and discussion

4.1. Simulation results and analysis of case 1

4.1.1. Flow field. Figure 2 shows the velocity distribution of the hot gas on the symmetry plane. The streamlines with arrows indicate the flow direction of the hot gas in the furnace. The hot gas runs along the negative direction of the x-axis. The greater the absolute value of the negative number, the greater running velocity of the hot gas is.

In Figure 2, the hot gas velocity in the higher areas is mainly concentrated in the middle of the preheating zone and the middle-upper part of the heat exchange zone. This is due to the flow resistance of the hot gas at the bottom of the preheating zone is large. The hot gas flows to the upper part of the preheating zone and the upper part of the heat exchange zone easily. Therefore, the flow velocity of the hot gas is larger. The lower-velocity areas are mostly concentrated in the top of the heating zone II and the top of the soaking zone. The reason is that the flow resistance of the hot gas near the furnace side wall is small. Under the action of the top pressure, the hot gas flows into the lower and both sides of the furnace.

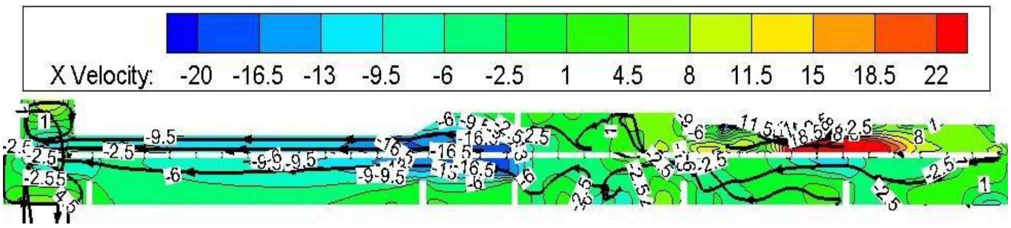

Figure 2. The velocity distribution of the hot gas on the symmetry plane in case1.

IOP Conf. Series: Earth and Environmental Science **467** (2020) 012025 doi:10.1088/1755-1315/467/1/012025

4.1.2. Pressure distribution. Figure 3 shows the pressure distributions along the furnace length direction at different locations on the zero pressure plane of the furnace. Line22 locates at the central axis. Along the width direction of the furnace, line23 is 1.5m away from the central axis of the furnace. Line24 and line25 are 3.0m and 4.5m away from the central axis of the furnace, respectively.

In Figure 3, from the heat exchange zone to the soaking zone, these curves display similar trends. In the heat exchange zone, these curves basically overlap each other. In the preheating zone, these curves are rising. However, the degree of change is different. Line22 and the line23 are sharply rising, while line24 and line25 are gently rising. In addition, pressure values of line22 and line23 are more than the pressure values of line24 and line25. This indicates that the pressure is higher at locations closer to the center axis of the furnace. The reason is that the flow resistance of the hot gas near the center axis of the furnace is larger. In the heating zone I, these curves rise first, then drop, and then rise again. The rise is due to the partition walls at the bottom of the furnace increase the flow resistance of the hot gas. The reason for the pressure drop is that after crossing the partition walls, the flow resistance of the hot gas decreases. However, it is worth noting here that the pressure near the central axis of the furnace is much higher than the pressure near the side walls of the furnace. The reason is that the side burners accelerate the flow of the hot gas toward the middle of the furnace and the amount of the hot gas at the middle of the furnace increases. The result is the flow resistance of the hot gas at the middle of the furnace greater than other locations. In the heating zone II and the soaking zone, these curves tend to be stable, due to the vertical pressure of the side burners offset the downward pressure of the top burners.

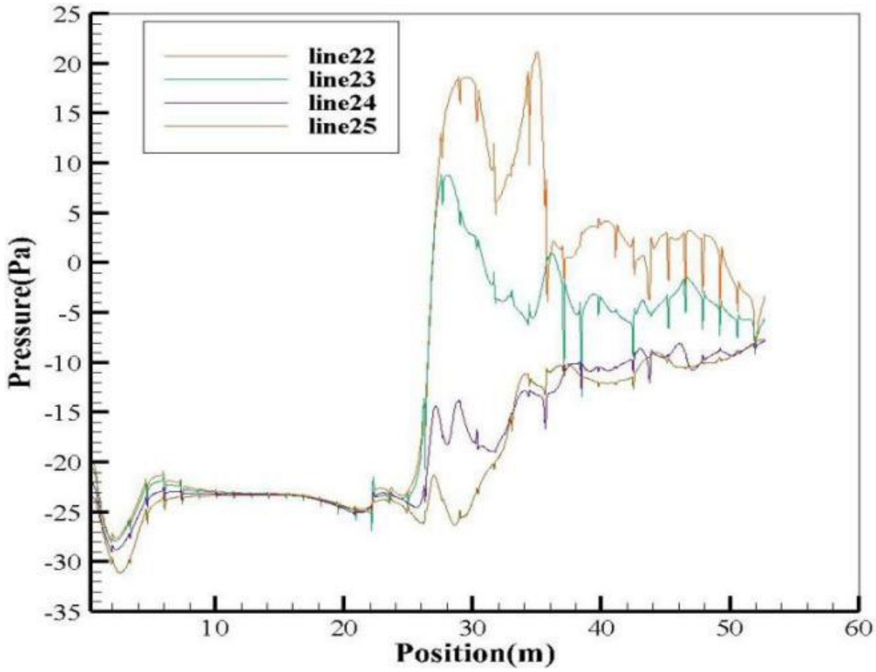

Figure 3. The pressure distributions along the furnace length at different locations on the zero pressure plane of the furnace in case1.

4.1.3. Analysis. In summary, the partition walls at the bottom of the preheating zone have a significant influence on the hot gas flow. These walls increase the pressure at the bottom of the preheating zone. Under this pressure, the hot gas at the bottom of the preheating zone flows into the middle-upper of the heat exchange zone and the preheating zone. This makes that the volume of the hot gas at the bottom of the preheating zone is less than that in the middle-upper part. Thereby a low-temperature zone is formed at the bottom of the preheating zone. The low-temperature zone affects the heating of the slab in the furnace, which makes the lower surface of the slab to gain less heat than the upper surface. Since the supported beams and the upright columns also have a shadow effect on the lower surface of the slab, which would lower surface of the slab in the heating exchange zone and the preheating zone can't get sufficient heating. As a result, there is a larger temperature difference between the upper surface and the lower surface of the slab. Since the pressure near the center axis of the furnace is the highest, the volume of the hot gas in the middle of the preheating zone bottom is the lowest. Thus, it can be seen that the temperature difference between the upper surface and the lower surface of the slab at this location is the largest and the maximum temperature difference appears to be in the preheating zone.

In order to eliminate the temperature difference between the upper surface and the lower surface and improve the reheating quality, it is necessary to increase the residence time of the slab in the furnace. However, increasing the residence time will increase fuel consumption and metal oxidation. This is detrimental to the energy saving of the reheating furnace and the improvement of the quality of the slab. Therefore, it is especially necessary to modify the partition walls in the preheating zone of the reheating furnace.

4.2. Test results and analysis of case 1

Figure 4, Figure 5 and Figure 6 show the temperature distributions through the slab thickness at three different location: the left end of the slab, the middle length of the slab, the right end of the slab, respectively. The total time of the experimental slab in the furnace is about 270min and the maximum temperature of the slab about is 1200℃. In addition, Figure 4 shows that the maximum temperature difference at the left end of the slab appears at 120min and the maximum temperature difference is about 260℃. Figure 5 shows that the maximum temperature difference at the middle length of the slab appears at 130min and the maximum temperature difference is about 310℃. Figure 6 shows that the maximum temperature difference at the right end of the slab appears at 120min and the maximum temperature difference is about 290℃. It can be seen that the middle length of the slab is the place where the temperature uniformity is the worst in the slab. This is in agreement with the simulation result in case1.

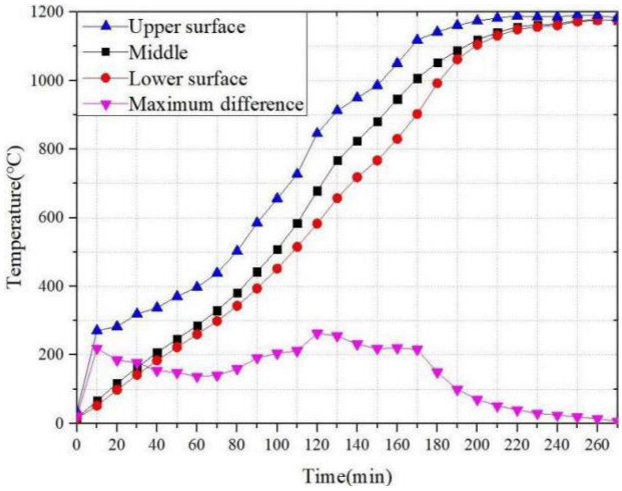

Figure 4. Temperature distribution at the slab left end in case 1.

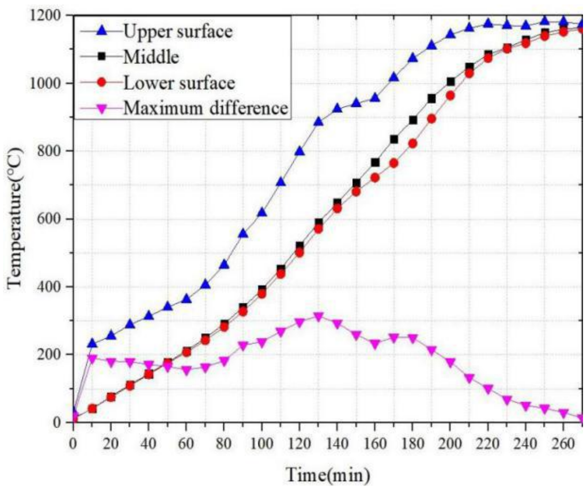

Figure 5. Temperature distribution at the middle of the slab in case1.

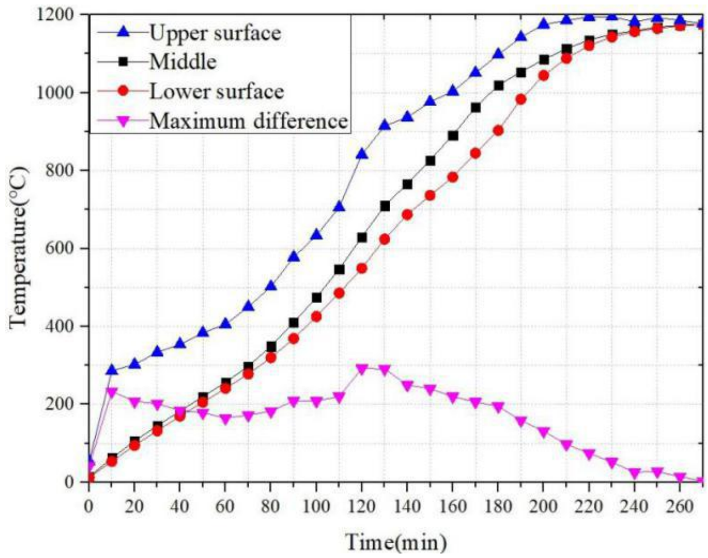

Figure 6. Temperature distribution at the right end of the slab in case1.

4.3. Simulation results and analysis of case 2

4.3.1. Flow field. Figure 7 shows the velocity distribution of the hot gas on the symmetry plane in case2. Since the middle partition wall at the bottom of the preheating zone was removed, the flow resistance of the hot gas becomes small, the middle-lower part of the preheating zone becomes the area of the highest velocity. The hot gas in the middle-upper part of the heat exchange zone still has a large velocity. Compared to Figure 2, however, the higher velocity zone of the heat exchange zone shown in Figure 7 can cover most slab's upper and lower surfaces. This ensures the slab in the heat exchange zone is fully heated. In addition, the lower-velocity areas of the heating zone II top and the soaking zone top disappear. The uniformity of the velocity distribution of the hot gas is improved. As a result, compared with that shown in Figure 2, the distribution of hot gas shown in Figure 7 is relatively uniform.

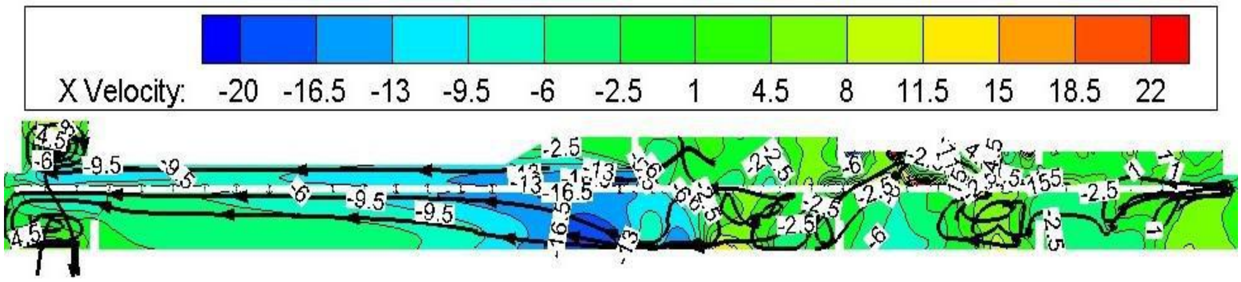

Figure 7. The velocity distribution of the hot gas on the symmetry plane in case2.

4.3.2. Pressure distribution. Figure 8 shows the pressure distributions along the furnace length direction at different locations on the zero pressure plane of the furnace. Line26 locates at the central axis. Along the width direction of the furnace, line27 is 1.5m away from the central axis of the furnace. Line28 and line29 are 3.0m and 4.5m away from the central axis of the furnace, respectively.

Figure 8 shows that the pressure uptrend near the central axis position in the preheating zone is significantly slower than the pressure uptrend in the preheating zone shown in Figure 3. The maximum pressure difference in the furnace is smaller than the maximum pressure difference shown in Figure 3. This indicates that furnace local resistance of the preheating zone after the bottom partition wall reconstruction is reduced; the flow condition of the hot gas is improved. In addition, the pressure in the heat exchange zone is increasing. The maximum pressure difference between the preheating zone and the heat exchange zone has been reduced. This suggests that the hot gas flows into the middle of the heat exchange zone more easily. The quantity of the hot gas in the middle of the heat exchange zone is increasing as shown in Figure 5. In the heating zone I, the pressure uptrend is slower than that shown in Figure 3. This indicates that the flow of hot gas toward the bottom and both sides of the furnace is weakened. The quantity of the hot gas at the top of the heating zone Ⅱ and the soaking zone has increased. The temperature of the top of the heating zone Ⅱ and the soaking zone has increased.

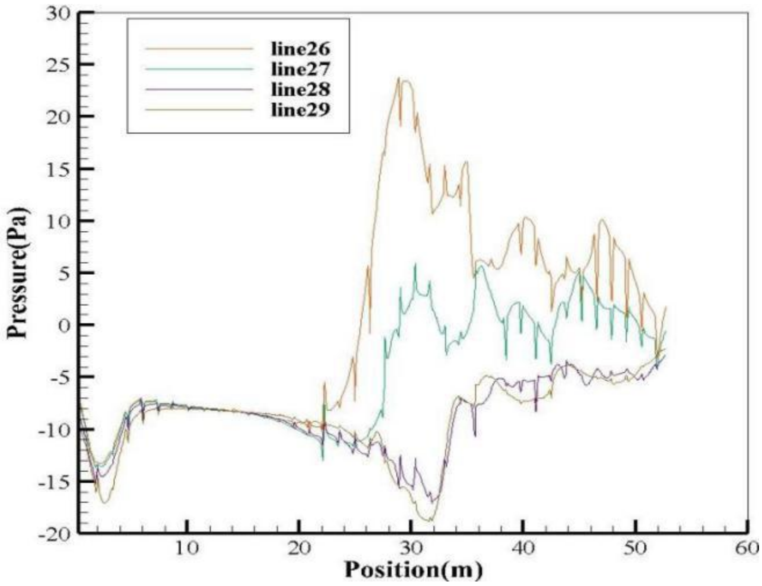

Figure 8. The pressure distributions along the furnace length direction at different locations on the zero pressure plane of the furnace in case2.

4.3.3. Analysis. To sum up, after the middle partition walls in the preheating zone are removed, the maximum pressure difference between the preheating zone and the heat exchange zone is decreased. The hot gas at the bottom of the preheating zone runs smoothly and the flow of the hot gas toward the middle-upper part of the preheating zone and the heat exchange zone is slowed down. The volume of the hot gas flows into the upper part of the heat exchange zone is decreased and flows into the middle of the heat exchange zone is increased. Thus, the upper surface and the lower surface of the most slabs are well covered by the hot gas. Additionally, the middle gap of the preheating zone partition wall increases the radiation of the high-temperature zone of the middle and lower of the furnace toward the low-temperature zone. These lead to that the lower surface in the middle of the furnace is well heated. Thus, both the temperature difference between the upper surface and the lower surface of the middle of the slab and the residence time of the slab in the furnace are reduced. Therefore, after the partition wall in the preheating zone is remodeled, the fuel consumption of the reheating furnace is reduced; product quality of the slab and heating efficiency of the reheating furnace are improved.

4.4. Test results and analysis of case 2

Figure 9 shows the temperature distribution at the middle of the experimental slab. The residence time of the experimental slab in the furnace is about 230min and the maximum temperature of the slab is about 1200°C. In comparison with case1, when the slab reaches the 1200°C, the slab in case2 has a shorter residence time in the furnace and the reheating furnace consumes less fuel in case2. Therefore, case2 is more energy efficient than case1. In addition, Figure 9 also shows that the maximum temperature difference in the middle of the slab appears at 110min and the maximum temperature difference is about 180℃. In comparison with the Figure 5 in case1, the maximum temperature difference in the middle of the slab is significantly reduced. This is in agreement with the simulation result in case 2.

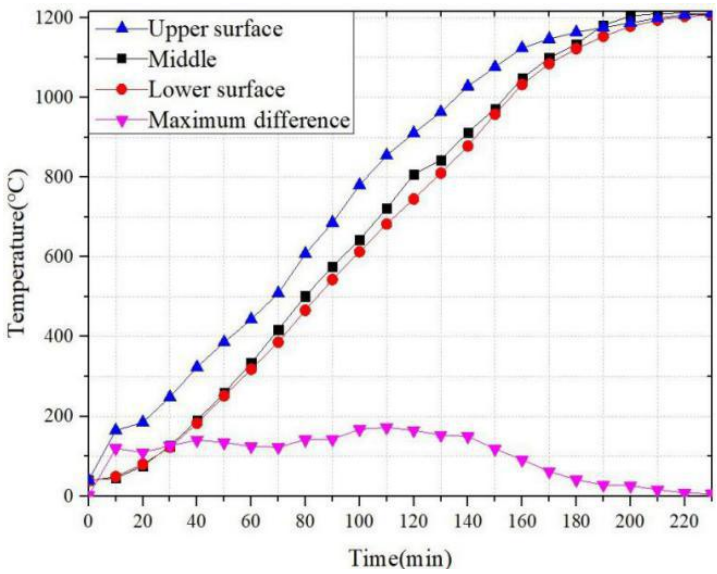

Figure 9. Temperature distribution at the middle of the slab in case 2.

5. Conclusions

In this study, the fluent software is used to analyze the pressure distribution in the walking beam reheating furnace and the following conclusions are obtained:

The partition wall in the preheating zone of the reheating furnace has a great influence on the pressure distribution. The pressure distribution in the furnace can be changed by retrofitting the bottom partition wall structure in the preheating zone. Thereby, the distribution of the hot gas and the temperature distribution in the furnace can be improved. A reasonable partition wall structure can improve the uniformity of the flow field and the temperature field in the furnace. Thus, the heating efficiency of the reheating furnace can be improved and the fuel consumption of the reheating furnace can be reduced. Hence, this provides a new method for energy-saving retrofitting of reheating furnaces.

In addition, by comparing the simulation result with the experimental result, it is feasible to use the simulation method to study the pressure distribution in the furnace, which also provides support for using the numerical simulation method to study the pressure distribution in the furnace.

References

[1] Han S H, Lee Y S, Cho J R, Lee K H 2018 Efficiency analysis of air-fuel and oxy-fuel combustion in a reheating furnace *Int J Heat Mass Tran* **121** 1364

[2] Han S H, Chang D, Huh C 2011 Efficiency analysis of radiative slab heating in a walking-beam-type reheating furnace *Energy* **36** 1265

[3] Jaklič A, Kolenko T, Zupančič B 2005 The influence of the space between the billets on the productivity of a continuous walking-beam furnace *Appl Therm Eng* **25** 783

[4] Han S H, Chang D 2012 Optimum residence time analysis for a walking beam type reheating furnace *Int J Heat Mass Tran* **55** 4079

[5] Lee D E, Kim M Y 2013 Optimum residence time for steel productivity and energy saving in a hot rolled reheating furnace *J Mech Sci Technol* **27** 2869

[6] Morgado T, Coelho P J, Talukdar P 2015 Assessment of uniform temperature assumption in zoning on the numerical simulation of a walking beam reheating furnace *Appl Therm Eng* **76** 496

[7] Jang J Y, Huang J B 2015 Optimization of a slab heating pattern for minimum energy consumption in a walking-beam type reheating furnace *Appl Therm Eng* **85** 313
[8] Jang J Y, Huang J B 2018 Optimisation of a slab heating pattern with various skid button heights in a walking-beam-type reheating furnace *Ironmak Steelmak* **45** 793
[9] Emadi A, Saboonchi A, Taheri M, et al 2014 Heating characteristics of billet in a walking hearth type reheating furnace *Appl Therm Eng* **63** 396
[10] Casal José Manuel, Porteiro J, Míguez José Luís, et al 2015 *Appl Therm Eng* **86** 69
[11] Liu G K, Chen Z C, Li Z Q, et al 2015 *Appl Therm Eng* **75** 1034
[12] García Alex M, Amell Andrés A 2018 *Int J Heat Mass Tran* **127** 1208
[13] Han S H , Chang D , Kim C Y 2010 *Int J Heat Mass Tran* **53** 3855
[14] Liu Y J , Li J D, Misra R D K, et al 2016 *Appl Therm Eng* **107** 1304
[15] FLUENT 6.3 User's Guide, Fluent Inc., Lebanon, USA, 2006